Electrical conductivity of ceria-based electrodes for use in magnetohydrodynamic generators

Michael Johnson[1,2], David Cann[1,2], Bryce Wright[1,2], Kyei-Sing Kwong[2], and C. Rigel Woodside[2]

[1]Materials Science, School of Mechanical, Industrial, and Manufacturing Engineering, Oregon State University

[2]U.S. Department of Energy, National Energy Technology Laboratory, 1450 SW Queen Ave, Albany, OR 97321

Abstract

Direct power extraction using magnetohydrodynamics (MHD) has the potential to increase the energy efficiency of chemical (i.e. combustion) to electrical energy conversion by enabling power plant operation at higher temperatures. A critical component within the system is the electrodes, which are used to extract the electrical power. The electrodes must be stable from 1800 – 2400 K, maintain electrical conductivities ≥ 1 S/m, and must resist electrochemical attack from seed materials such as potassium. This work will focus on ceria-based ceramic electrodes developed for use in MHD power systems. Ceramic disks of undoped CeO_2 as well as Y_2O_3- and Gd_2O_3-doped CeO_2 were synthesized using solid state processing techniques. The sintered ceramics were analyzed via x-ray diffraction, and the electrical properties were measured through impedance spectroscopy and DC current-voltage measurements. In addition, electrochemical potential experiments were conducted to determine the role of ionic conductivity in these materials. Overall, the doped CeO_2 ceramics exhibited an increase in conductivity with values approaching 10 S/m at 1500 K, with electronic conductivity dominating in the doped compositions. Corrosion tests also indicated these materials are relatively inert in the presence of K_2CO_3 up to 1500°C. Overall, these tests suggest that ceria-based ceramic electrodes show promise for use in MHD power systems.

Introduction

Research and development focused on direct power extraction using magnetohydrodynamics (MHD) is motivated by the fact that this technology can provide a significant increase in energy efficiency for chemical to electrical energy conversion by enabling the operation of power plants at higher temperatures. By utilizing high temperature gasses as a working fluid in a MHD topping unit, a combined-cycle coal-fired power plant can be expected to have plant thermal efficiencies close to 60% [1]. While the thermodynamic advantages of a MHD system have been established for a number of years, legacy US Department of Energy (DOE) research was impeded by challenges in the supporting technology. Fortunately, technologies such as advanced magnets and high temperature materials have improved greatly since previous DOE research efforts, making MHD a more viable option. Moreover, more recent interest in oxy-fuel combustion and carbon capture [2] has made MHD a more relevant technology because of the high temperature nature of the system. Thus, implementation of this technology has the potential to significantly reduce fossil fuel consumption and reduce greenhouse gas emissions.

A critical supporting technology for MHD is the high temperature materials which line the power extraction region. It is anticipated that the temperature of the exhaust gases can be as high as 3000 K with liner temperatures approaching 1800 K if there is coal slag, and temperatures between 1800 and 2400 K if there is no slag. One of the most critical components within the system is the electrodes, which are used to extract the electrical power. Historically, the electrodes have been metallic and water-cooled to values near 500 – 800 K. Such cooling creates severe temperature gradients and decreases the overall efficiency of the system. Thus, there is a need to develop electrodes which function at temperatures up to 2400 K. The

development of high temperature electrodes represents a critical enabling technology for the viability of high performance MHD systems.

The materials for use as high temperature electrodes should possess the following characteristics for effective implementation in MHD systems. First, the electrodes must be thermally stable over temperature ranges between 1800 – 2400 K. Second, electrical conductivity values greater than 1 S/m are needed over approximately that same temperature range. Finally, the ceramic electrodes must resist electrochemical attack from the slag or seed materials such as potassium.

Past research efforts on the development of ceramic electrodes for MHD systems focused on a number of different ceramic material systems. These include ZrO_2, Zr-containing perovskite materials (e.g. $BaZrO_3$ and $SrZrO_3$), HfO_2-based materials, chromate materials such as $LaCrO_3$, and rare earth zirconate materials such as $Ce_2Zr_2O_7$ [3-5]. While the ZrO_2-based systems have some advantageous properties, in particular chemical stability and electrical conductivity, there are concerns about the corrosion resistance in the presence of K. The $LaCrO_3$-based materials have excellent conductivity values, but the corrosion resistance has not been examined as there are concerns over the toxicity of the Cr component.

This work is focused on the synthesis and characterization of CeO_2-based materials for use as MHD electrodes. A significant amount of research has been conducted on these materials for their potential use as catalysts, steam reforming, and as electrolytes in solid oxide fuel cell systems. The oxide CeO_2 possesses the fluorite structure with space group *Fm3m* and retains that structure up to its melting point near 2750 K. This work explores two binary systems with CeO_2, incluing CeO_2-Y_2O_3 and CeO_2-Gd_2O_3. The oxide Y_2O_3 is stabilized in the C-type rare Earth structure with a melting temperature of 2698 K. Limited information about the phase

diagram for the CeO_2-Y_2O_3 system is known. It is characterized three solid phases at temperatures below 1500°C, including the cubic fluorite phase for compositions rich in CeO_2, the cubic C-type rare Earth structure for compositions rich in Y_2O_3, and for compositions between approximatley 30 to 70 mol% Y_2O_3 these two phases co-exist. The oxide Gd_2O_3 can be stabilized in either the monoclinic B-type or cubic C-type rare Earth structure and has a melting temperature of 2693 K. There is no phase diagram information on the CeO_2-Gd_2O_3 system, but a similar behavior would be expected given that Gd^{3+} and Y^{3+} are similar in size and electronic structure. Overall, the melting temperatures for compositions in these binary systems are well above the expected operating temperatures for MHD systems.

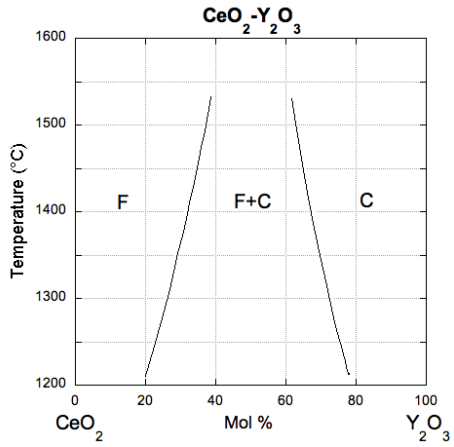

Figure 1. Phase equilibria diagram for CeO_2-Y_2O_3 (adapted from Jasper's slides – needs primary reference)

Another requirement of MHD electrodes is that they require electrical conductivity values greater than 1 S/m at temperatures between 1800 – 2400 K. At these extreme temperatures, charge carriers are expected to be generated from a multitude of mechanisms, including thermal excitation across the band gap as well as due to defects which should be present in high concentrations. Experimental measurements for the electronic band gaps for the

oxides CeO_2, Y_2O_3 and Gd_2O_3 are in the range of 5.4 to 6.0 eV. For band gaps in this range, the number of charge carriers at these temperatures is significant. Typically, materials with smaller band gaps are unsuitable due to lower melting temperatures or chemical instability.

Overall, these two binary systems, CeO_2-Y_2O_3 and CeO_2-Gd_2O_3, have favorable characteristics for meeting the basic requirements for high temperature electrical conductors. It is the purpose of this paper to synthesize compositions in these two binary systems and characterize their crystal structure, electronic properties and corrosion resistance to evaluate their suitability for use as electrode materials in MHD systems.

Experimental methods

All ceramics were prepared using a conventional solid-state method. Powders were produced by mixing the approiate stoichiometric amounts of binary oxides and then milled using a vibratory mill for 6 hours. The mixed powders were calcined at 1400°C for 6 hours, then milled again to reduce the particle size. The powders were then pressed into green pellets by cold pressing with a hydralic press by applying approximately 3 tons of force. The pellets were then sintered for 30 hr at 1600°C. The sintered pellets were found to have densities that varied based on their composition, but all were sintered to at least 85% of their theoretical density[3]. Once sintered, the pellets were polished and then had Pt electrodes applied on both faces of the sample. All measurements were conducted in a high temperature measurement cell (NorECs AS Probostat^{TM}, Norway). Impedance spectroscopy was conducted using an impedance analyzer (Solartron SI1260A along with a Solartron 1296A dielectric interface) and SMaRT software to collect measurements at frequencies ranging from 100 mHz to 1 MHz. The phase equilibria of the ceramics was investigated through the use of x-Ray diffraction (Bruker AXS D8 Discover).

To further understand the electrical characteristics of the MHD electrode, experiments were conducted to determine the conduction mechanism for the materials investigated in this study. Electromotive force (EMF) measurements were conducted utilizing the ProboStat by flowing laboratory air over one side of the sample and 99.9% oxygen over the other side. The aim of this experiment is to gauge the amount of oxygen-driven ionic conduction that occurs within a particular electrode material. This is done by measuring the ionic transport number, which is the fraction of the electrical conductivity of the material that is carried by an ionic species. The ionic transport number can be calculated through the Nernst equation[23],

$$V_m = \frac{RTt_i}{4F} ln \left|\frac{P_1}{P_2}\right| \quad (1)$$

where V_m is the voltage measured across the sample, R is the gas constant, T is the temperature, F is the Faraday constant and t_i is the ionic transport number. In this case, P_1 and P_2 are the oxygen pressures on each side of the sample, which were assumed to be 0.2 atm for the side exposed to air and 1 atm for the side exposed to the oxygen. While these assumptions are likely accurate at room temperature, the pressures could deviate from this at higher temperatures, causing the accuracy of assumptions to come into question. Due to these concerns, the ionic transport numbers received from this measurement should be considered qualitatively; they should be used to compare the amount of ionic conduction within the sample relative to the other samples examined in this study.

Results

Figure 2a shows the XRD data for sintered ceramics in the CeO_2-Y_2O_3 system. As expected from the phase diagram in Figure 1, pure CeO_2 possesses the fluorite structure, and as the Y_2O_3 mole fraction increases the structure slowly transitions to the cubic C-type rare earth

structure. Recent reports have found that small amounts of Y_2O_3 doping lead to the lattice constant of the fluorite to shrink slightly.[24] Similarly, Fig. 2b shows XRD patterns for ceria doped with different amounts of Gd_2O_3. The patterns closely match the previous results reported by Grover and Tyagi[7], where ceria transitions from the cubic fluorite structure to the cubic C-type rare earth, and then eventually into a monoclinic B-type structure as the mole fraction of Gd_2O_3 increases.

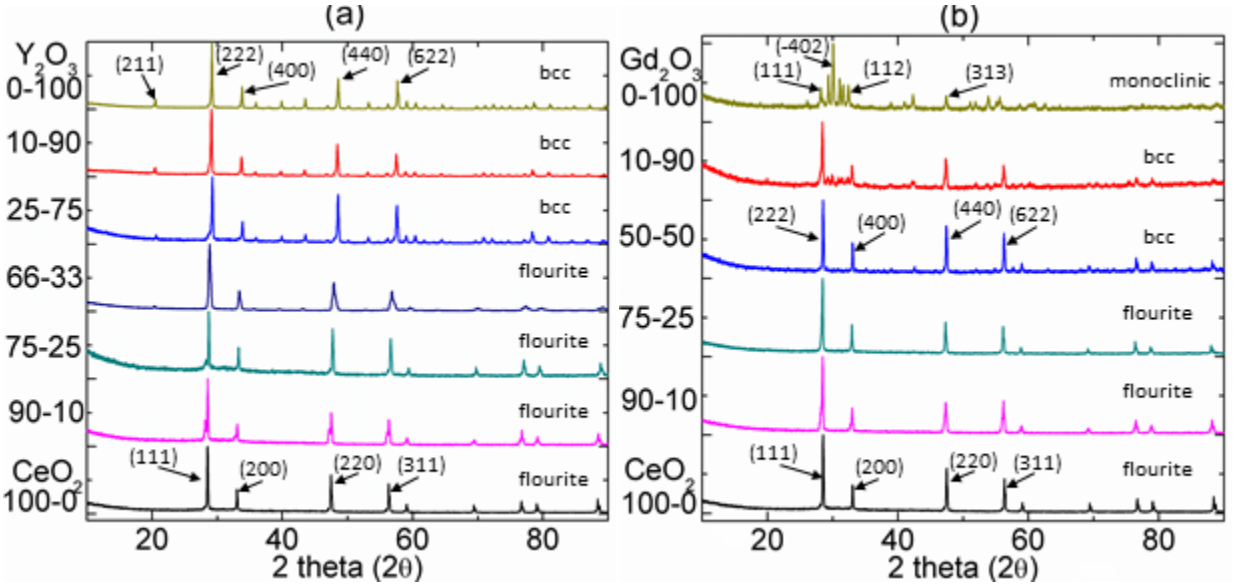

Figure 1. XRD patterns of compounds with different amounts of (a) Y_2O_3 and (b) Gd_2O_3 mixed with ceria. The ratios on the plots corresponded to the relative molar percent of ceria to the dopant. (Note: bcc refers to a body-centered cubic crystal structure)

The electrical conductivity of each of the samples was measured using impedance spectroscopy at temperatures ranging from 873 to 1450 K. Figure 3a shows the complex plot of pure ceria, along with ceria doped with 10 mol% Y_2O_3 in Fig. 3b and ceria doped with 10 mol% Gd_2O_3 in Fig. 3c. All of the spectra show evidence of electrical heterogeneity. This is likely due to microstructural effects such as the grain boundaries, or as will be discussed the presence of ionic conducting species. Most notably, ceria doped with 10 mol% Y_2O_3 had a much lower resistivity than the pure ceria, whereas ceria doped with 10 mol% Gd_2O_3 increased the resistivity by almost

an order of magnitude. To determine the origin of these large changes in resistance between the different compositions, an equivalent circuit analysis was utilized (Fig. 2d) to represent the discrete contributions to the impedance. Table 1 displays the different parameters assigned to each of the components within the equivalent circuit model for each of the compositions. Within this data set, the source of the resistivity can be approximated by the capacitance used within a typical equivalent circuit model, where R1 represents the instrument resistance, R_2 and C_2 represent the bulk contributions to the impedance, and R_3 and C_3 represent contributions to the impedance from the grain boundary.[25] The ceria doped with 10 mol% Gd_2O_3 likely had a much larger grain boundary resistance based upon the equivalent circuit, judging from the large value for R_3. The ceria doped with 10 mol% Y_2O_3 showed a much lower grain boundary resistance than the pure ceria, which is in good agreement with the findings of Tian and Chan[10].

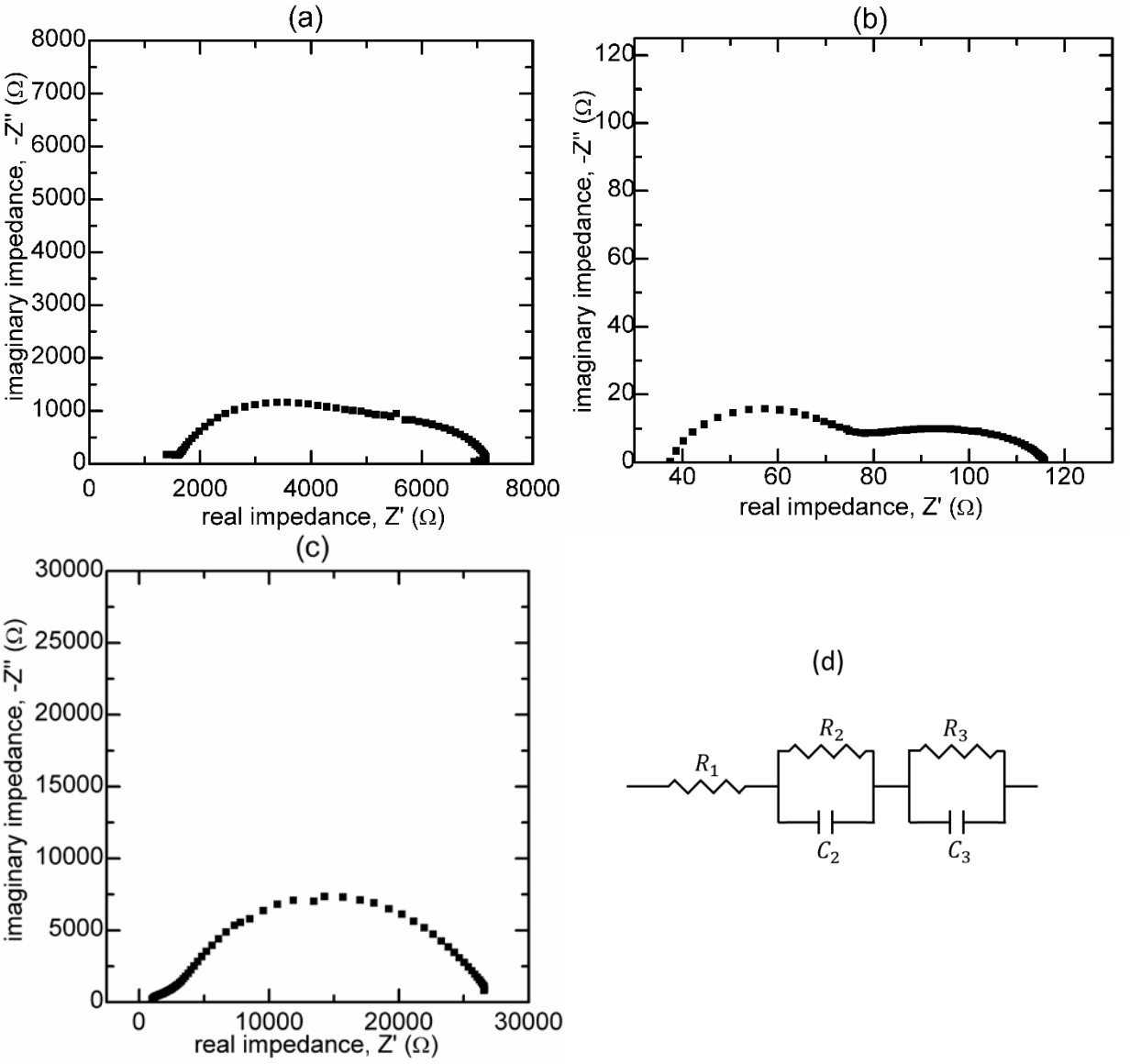

Figure 3. Complex plane plots of (a) pure CeO_2 (b) CeO_2-Y_2O_3: 90-10 mol% and (c) CeO_2-Gd_2O_3: 90-10 mol% at 873 K. All samples were cylindrical with a diameter of 11.2 mm and a thickness of 2.1 mm. (d) A model RC circuit used to approximate the electrical characteristics.

TABLE 1: PARAMETERS USED TO MODEL ELECTRICAL CHARACTERISTICS OF CERIA WITH DIFFERENT AMOUNTS OF DOPING

	R_1 (Ω)	R_2 (Ω)	C_2 (F)	R_3 (Ω)	C_3 (F)
CeO_2	600	800	8×10^{-11}	5500	1.5×10^{-8}
CeO_2-Y_2O_3: 90-10	35	40	1×10^{-6}	40	4.5×10^{-8}
CeO_2-Gd_2O_3: 90-10	600	1000	1×10^{-8}	25000	8.6×10^{-8}

To be a viable electrode for an MHD channel, the electrode needs to have sufficient electrical conductivity at temperatures approaching 2000 K. To determine how different mole fraction of the Y_2O_3 and Gd_2O_3 additives affect the electrical conductivity at high temperatures, the electrical conductivity of each sample was measured over a range of temperatures. The data set is not ideal as the samples had some level of porosity which undoubtedly affected the measurements. Nontheless, the results are useful as a preliminary assessment of the electrical conductivity of the materials in this study.

An Arrhenius plot of different compositions in the CeO_2-Y_2O_3 system is shown in Fig. 4a. As is indicated in the data, a clear divide emerges as samples with a large mole fraction of ceria have significantly higher conductivity values. Figure 4b shows the electrical conductivity of ceria doped with different mole fractions of Gd_2O_3. Interestingly, intermediate amounts of dopants, such as CeO_2-Y_2O_3 90-10 and CeO_2-Gd_2O_3 75-25, have higher conductivities at temperatures < 1600 K than pure ceria. This matches findings by Tianshu *et al.*[26], who showed that an intermediate amount of Gd_2O_3 in ceria produced the highest conductivities over the temperature range 400°C to 800°C. This was attributed to the effects of moderate (< 30 mol%) concentrations of Gd_2O_3 which decreased the activation energy of ceria. While Tianshu *et al.*[26] only studied this behavior in CeO_2-Gd_2O_3, it appears these trends are also true for the CeO_2-Y_2O_3 compositions. However, the activation energies of both $90CeO_2$-$10Y_2O_3$ and $75CeO_2$-$25Gd_2O_3$ appear to increase at higher temperatures, causing it to exhibit a non-linear behavior on the Arhenious plots. Tables 2 and 3 show the linear fit parameters of the different mixtures for CeO_2-Y_2O_3 and CeO_2-Gd_2O_3, respectively, along with the predicted electrical conductivity of each of the materials at 2000 K. Pure ceria is predicted to have the highest conductivity at 2000 K due to the compositions $90CeO_2$-$10Y_2O_3$ and $75CeO_2$-$25Gd_2O_3$ having activation energies that increased with temperature.

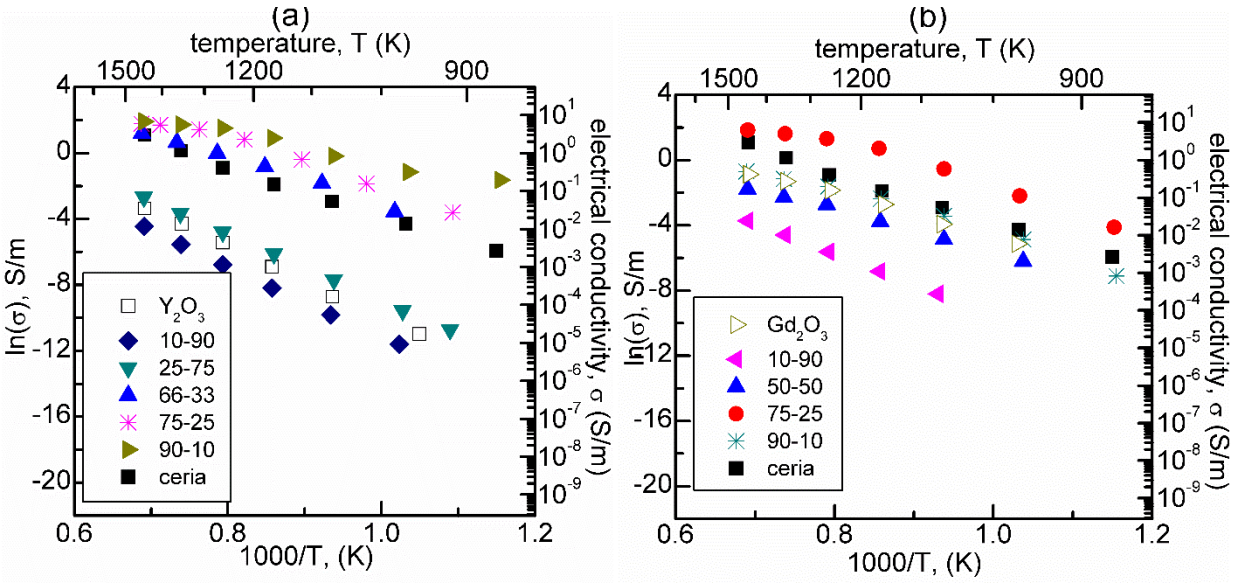

Figure 3. An Arrhenius plot of the electrical conductivity of ceria with different amounts of (a) Y_2O_3 and (b) Gd_2O_3 at different temperatures.

TABLE 2. ELECTRICAL CONDUCTIVITY DATA FOR CeO_2-Y_2O_3 COMPOUNDS AND FITTING PARAMETERS FROM ARRHENIUS ANALYSIS

	σ (S/m) (T=1400 K)	σ_o	E_a (eV)	Extrapolated conductivity at T=2000 K (S/m)
Y_2O_3		116300	1.86	2.33
CeO_2 - Y_2O_3 10-90		75700	1.96	14.7
CeO_2 - Y_2O_3 25-75		89100	1.76	3.34
CeO_2 - Y_2O_3 66-33		25100	1.11	39.2
CeO_2 - Y_2O_3 75-25		8880	0.89	14.7
CeO_2 - Y_2O_3 90-10		419	0.51	0.65
CeO_2		76270	1.30	85.2

TABLE 3. ELECTRICAL CONDUCTIVITY DATA FOR CeO_2-Gd_2O_3 COMPOUNDS AND FITTING PARAMETERS FROM ARRHENIUS ANALYSIS

	σ (S/m) (T=1400 K)	σ_o	E_a (eV)	Extrapolated conductivity at T=2000 K (S/m)
Gd_2O_3		2840	1.08	3.52
CeO_2-Gd_2O_3 10-90		9770	1.61	0.85
CeO_2-Gd_2O_3 50-50		571	1.01	2.07
CeO_2-Gd_2O_3 75-25		237	0.45	17.2
CeO_2-Gd_2O_3 90-10		421	0.84	3.2

CeO_2		76300	1.30	85.2

Cerium oxide can exhibit electronic conduction, ionic conduction, or mixed conduction based upon the oxygen partial pressure, temperature and dopant. Oxygen non-stoichiometry is observed through the reduction reaction as follows (Mogensen):

$$O_O + 2Ce_{Ce} = \tfrac{1}{2}O_{2(gas)} + V_O^{\bullet\bullet} + 2Ce'_{Ce} \qquad [1]$$

As a consequence, the oxygen vacancy concentration is dependent upon the oxygen partial pressure. Assuming non-interacting defects, the oxygen vacancy concentration should vary as:

$$[V_O^{\bullet\bullet}] = Constant \cdot pO_2^{-1/6} \qquad [2]$$

Oxygen non-stoichiometry may also result from doping, such as the addition of Y_2O_3 and Gd_2O_3, as follows:

$$Gd_2O_3 = 2Gd'_{Ce} + V_O^{\bullet\bullet} + 3O_O \qquad [3]$$

$$Y_2O_3 = 2Y'_{Ce} + V_O^{\bullet\bullet} + 3O_O \qquad [4]$$

From Vinokurov *et al.*, CeO_2 is generally regarded as an n-type conductor over the temperature range 200 to 1300°C, with primarily n-type small polaron conduction and a small fraction of oxide ion conduction, depending upon the temperature and pO_2.

Ionic conductivity within ceria is linked to the level of oxygen non-stoichiometry which can lead to an increase in ionic diffusion within the lattice. Figure 5 illustrates the compositional dependence of the ionic transport number at 1073 K for CeO_2-Y_2O_3 and CeO_2-Gd_2O_3.The concentration of oxygen vacancies can be increased though the addition of dopants with lower valence ions such as shown in equations 3 and 4[27]. This results in an increase in ionic transport

number for dopant concentrations < 20 mol%[28]. This is shown in Fig. 5a and b, where the transference number increased with the addition of both Y_2O_3 and Gd_2O_3. As the mole fraction of both Y_2O_3 and Gd_2O_3 increased further, the ionic transport number decreased which matches with results reported in the literature[29].

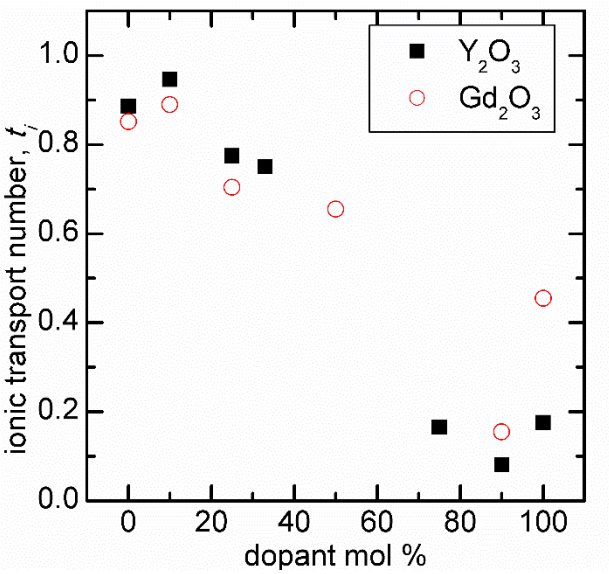

Figure 5. The measured transference number of CeO_2 with different amounts of Y_2O_3 and Gd_2O_3 at 1073 K.

Figure 6 presents the temperature dependence of the ionic transport number for compositions in the binary systems CeO_2-Y_2O_3 and CeO_2-Gd_2O_3. At higher temperatures, the level of oxygen non-stoichiometry increases through the reduction reaction shown in equation 1. The level of oxygen non-stoichiometry in the chemical formula CeO_{2-x}, can vary between $0 \leq x \leq 0.35$.[30] This strongly affects the ionic conductivity within ceria, as the reduction of oxygen leads to increased ionic mobility within the material, thus producing higher ionic conductivities. Figure 6 shows that compositions rich in CeO_2 are primarily electronic conductors at lower temperatures and transition into ionic conductors as the temperature approaches 1100 K.

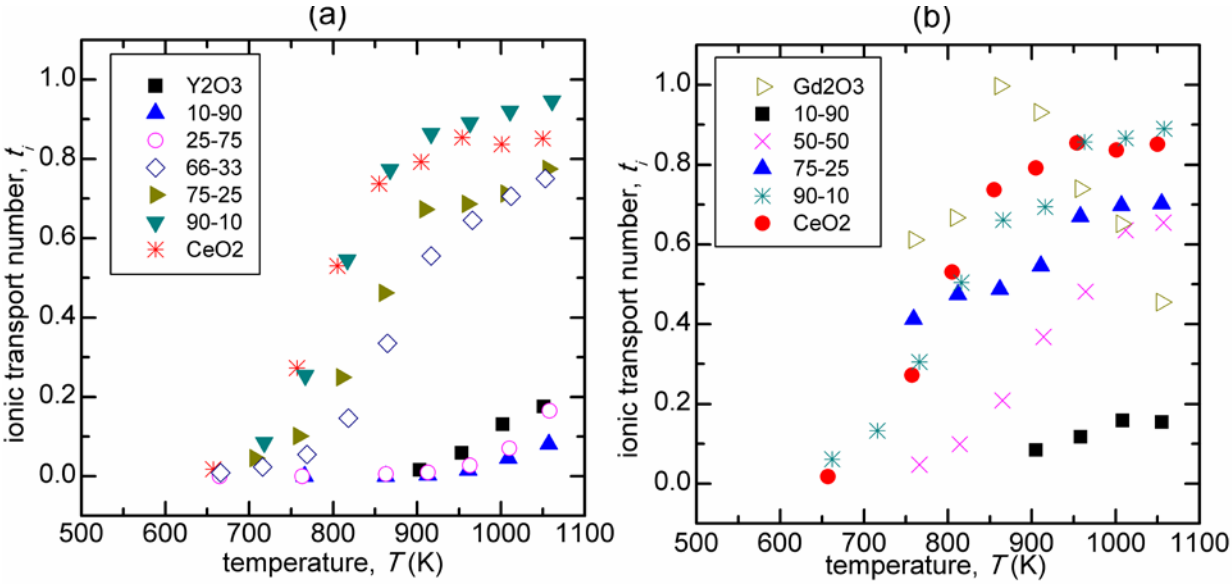

Figure 6. The ionic transport number of ceria doped with different amount of (a) Y_2O_3 and (b) Gd_2O_3 at different temperatures.

Another consideration for viable MHD electrode materials is that they must withstand the corrosive effects of the potassium plasma that will be used within the working fluid. To investigate possible reaction pathways between the electrode material and the potassium plasma, CeO_2, Y_2O_3 and Gd_2O_3 powders were mixed with K_2CO_3, pressed into a green body, then fired in a tube furnace at 1500°C for 1 hour. In addition, ZrO_2 powder was included in this study as a reference material. After firing, the samples were ground into a fine powder and evaluated through XRD. While this approach does not fully mimic the high temperature, high velocity environment within the MHD channel which likely enhances corrosion effects, it is still useful as a preliminary test to identify any possible reaction products from the electrode material and potassium. The results from this study are shown in Fig. 7 for the four different oxides. As shown in the XRD data, the CeO_2, Y_2O_3 and Gd_2O_3 specimens did not show any signs of potassium reaction. This is not a definitive test because it is possible that transient K-containing product phases may have formed and volatilized during the test leaving behind no evidence in the XRD pattern. Similarly, it is possible that amorphous or poorly crystalline phases were formed that were not detectable by XRD.

Tests on ZrO_2 produced the $K_2Zr_2O_5$ phase which was identifiable via XRD presumably through reaction with the potassium carbonate. The peaks indicated on Fig. 7d are peaks found in $K_2Zr_2O_5$ [31], indicating that it was formed as a byproduct during the test. This is an interesting result, as ZrO_2 has been commonly used as electrodes in many previous MHD channels, which could explain some previous corrosion issues[32, 33]. From this preliminary test, CeO_2, Y_2O_3, and Gd_2O_3 did not show any signs of reaction with K_2CO_3, which suggests they may be able to withstand the corrosive environment within a MHD channel. Future corrosion tests will expose the electrode materials to conditions closer to operating conditions.

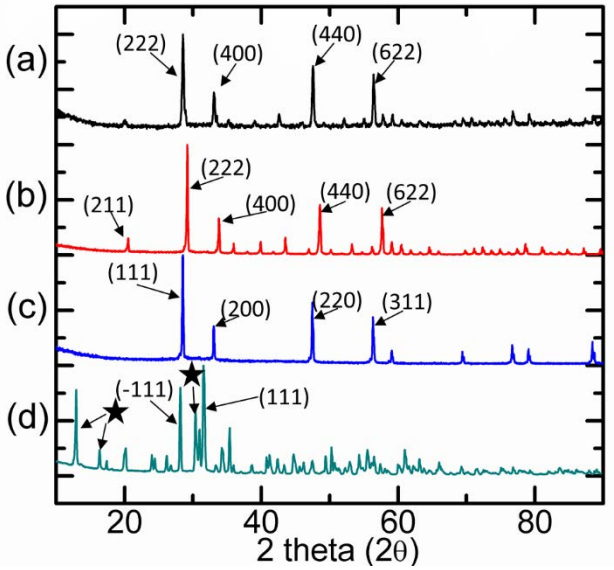

Figure 6. XRD patterns taken from (a) Gd_2O_3 (b) Y_2O_3 (c) CeO_2 and (d) ZrO_2 powders that were mixed with K_2CO_3, pressed into green bodies and then fired at 1773 K for 1 hour. Peaks marked with a ★ can likely be attributed to the formation of $K_2Zr_2O_5$.

Conclusions

In this work, CeO_2-Y_2O_3 and CeO_2-Gd_2O_3 based ceramics were evaluated for use as electrodes in MHD power extraction systems. Impedance spectroscopy measurements showed compositions rich in CeO_2 showed high conductivity values approaching 10 S/m at temperatures

above 1500 K. Electrochemical potential experiments were conducted and it was determined that at low temperatures electronic conductivity dominated and transitioned into an ionic conduction mechanism as temperatures above 900 K. This increase in ionic conductivity was attributed to increased oxygen non-stoichiometry at high temperatures. To assess the electrode materials resistance to chemical attack from seed materials such as potassium, specimens were annealed in a K_2CO_3 environment at 1500°C for 1 hour. The results showed that CeO_2, Y_2O_3, and Gd_2O_3 did not show any signs of reaction with K_2CO_3. Overall, these tests suggest that ceria-based ceramic electrodes show promise for use as electrodes in MHD power systems.

References

1 N.S. Jacobson, "Thermodynamic properties of some metal oxide-zirconia systems," *NASA Tech. Memo.*, **102351** 1–64 (1989).

2 K.J. Lesker, *Cerium Oxide (CeO2) Pieces Evaporation Materials*, (2017).

3 M. Mogensen, N.M. Sammes, and G.A. Tompsett, "Physical, chemical and electrochemical properties of pure and doped ceria," *Solid State Ionics,* **129** [1] 63–94 (2000).

4 F.S. Brugner and R.N. Blumenthal, "Electrical Conductivity of Single Crystal CeO2," *J. Am. Ceram. Soc.*, **54** [1] 57–57 (1971).

5 W. Noddack and H. Walch, "Conductivitty Measurements on Rare Earth Metal Oxides: II," *Z. Phys. Chem.*, **211** 194–207 (1959).

6 T.A.C. Society, "Phase Equilibria Diagrams;" in *Phase Equilibria Diagrams*. The American Ceramic Society, Westerville, Ohio 43082, n.d.

7 V. Grover and A.K. Tyagi, "Phase relations, lattice thermal expansion in CeO2–Gd2O3 system, and stabilization of cubic gadolinia," *Mater. Res. Bull.*, **39** [6] 859–866 (2004).

8 N.M. Tallan and R.W. Vest, "Electrical Properties and Defect Structure of Y2O3," *J. Am. Ceram. Soc.*, **49** [8] 401–404 (1966).

9 T. Norby and P. Kofstad, "Electrical Conductivity of Y2O3 as a Function of Oxygen Partial Pressure in Wet and Dry Atmospheres," *J. Am. Ceram. Soc.,* **69** [11] 784–789 (1986).

10 C. Tian and S.W. Chan, "Ionic conductivities, sintering temperatures and microstructures

of bulk ceramic CeO2 doped with Y2O3," *Solid State Ionics*, **134** [1–2] 89–102 (2000).

[11] D.Y. Wang, D.S. Park, J. Griffith, and A.S. Nowick, "Oxygen-ion conductivity and defect interactions in yttria-doped ceria," *Solid State Ionics*, **2** [2] 95–105 (1981).

[12] S. Jeon and H. Hwang, "Effect of hygroscopic nature on the electrical characteristics of lanthanide oxides (Pr2O3, Sm2O3, Gd2O3, and Dy2O3)," *J. Appl. Phys.*, **93** [10 1] 6393–6395 (2003).

[13] Chul Hyun Yo, Cheol Woo Kim, Eun Seok Lee, Woong Bum Pyon, and Jae Shi Choi, "A study of the nonstoichiometry and electrical conductivity of gadolinium sesquioxide," *J. Phys. Chem. Solids*, **49** [7] 835–839 (1988).

[14] C. Artini, G.A. Costa, M. Pani, A. Lausi, and J. Plaisier, "Structural characterization of the CeO 2/Gd 2O 3 mixed system by synchrotron X-ray diffraction," *J. Solid State Chem.*, **190** 24–28 (2012).

[15] D.K. Hohnke, "Ionic conduction in doped oxides with the fluorite structure," *Solid State Ionics*, **5** [C] 531–534 (1981).

[16] S. Maschio, O. Sbaizero, and S. Meriani, "Mechanical properties in the ceria-zirconia system," *J. Eur. Ceram. Soc.*, **9** [2] 127–132 (1992).

[17] N. Sammes, G. Tompsett, Y. Zhang, A. Cartner, and R. Torrens, "The structural and mechanical properties of (CeO2) 1-X (GdO1.5) X electrolytes," *Denki Kagaku*, **64** [6] 674–680 (1996).

[18] E.W. Awin, S. Sridar, R. Shabadi, and R. Kumar, "Structural, functional and mechanical properties of spark plasma sintered gadolinia (Gd2O3)," *Ceram. Int.*, **42** [1] 1384–1391 (2016).

[19] A.A. Kaminskii, M.S. Akchurin, R. V. Gainutdinov, K. Takaichi, A. Shirakava, H. Yagi, T. Yanagitani, and K. Ueda, "Microhardness and fracture toughness of Y2O3-and Y3Al5O12-based nanocrystalline laser ceramics," *Crystallogr. Reports*, **50** [5] 869–873 (2005).

[20] V. Dimitrov and T. Komatsu, "An interpretation of optical properties of oxides and oxide glasses in terms of the electronic ion polarizability and average single bond strength," *J. Univ. Chem. Technol. Met.*, **45** [3] 219–250 (2010).

[21] X. Zhao, X. Wang, H. Lin, and Z. Wang, "Electronic polarizability and optical basicity of lanthanide oxides," *Phys. B Condens. Matter*, **392** [1–2] 132–136 (2007).

[22] T.S. Zhang, J. Ma, L.B. Kong, S.H. Chan, and J.A. Kilner, "Aging behavior and ionic conductivity of ceria-based ceramics: A comparative study," *Solid State Ionics*, **170** [3–4] 209–217 (2004).

[23] Y. Hirata and M. Matsuda, "Composition Dependence of Electromotive Force of Silica-Alumina Ceramics as Oxygen Solid Electrolyte," *J. Ceram. Soc. Japan*, **102** [1183] 241–246 (1994).

[24] J. van Herle, T. Horita, T. Kawada, N. Sakai, H. Yokokawa, and M. Dokiya, "Sintering

behaviour and ionic conductivity of yttria-doped ceria," *J. Eur. Ceram. Soc.*, **16** [9] 961–973 (1996).

[25] J.T.S. Irvine, D.C. Sinclair, and A.R. West, "Electroceramics: Characterization by Impedance Spectroscopy," *Adv. Mater.*, **2** [3] 132–138 (1990).

[26] Z. Tianshu, "Ionic conductivity in the CeO2–Gd2O3 system (0.05≤Gd/Ce≤0.4) prepared by oxalate coprecipitation," *Solid State Ionics*, **148** [3–4] 567–573 (2002).

[27] M. Mogensen, "Physical Properties of Mixed Conductor Solid Oxide Fuel Cell Anodes of Doped CeO_2," *J. Electrochem. Soc.*, **141** [8] 2122 (1994).

[28] G. Balazs, "ac impedance studies of rare earth oxide doped ceria," *Solid State Ionics*, **76** [1–2] 155–162 (1995).

[29] S.P.S. Badwal, D. Fini, F.T. Ciacchi, C. Munnings, J.A. Kimpton, and J. Drennan, "Structural and microstructural stability of ceria – gadolinia electrolyte exposed to reducing environments of high temperature fuel cells," *J. Mater. Chem. A*, **1** [36] 10768 (2013).

[30] B. Bulfin, A.J. Lowe, K.A. Keogh, B.E. Murphy, O. Lübben, S.A. Krasnikov, and I. V. Shvets, "Analytical model of CeO2 oxidation and reduction," *J. Phys. Chem. C*, **117** [46] 24129–24137 (2013).

[31] B.M. Gatehouse and D.J. Lloyd, "The crystal structure of beta-potassium dizirconate: β-K2Zr2O5," *J. Solid State Chem.*, **1** [3–4] 478–483 (1970).

[32] N. Kayukawa, *Open-cycle magnetohydrodynamic electrical power generation: A review and future perspectives*, *Prog. Energy Combust. Sci.*, **30** [1] 33–60 (2004).

[33] R. Kessler, "Magnetohydrodynamics;" in *Kirk-Othmer Encycl. Chem. Technol.* John Wiley & Sons, Inc., Hoboken, NJ, USA, 2000.